Steel and Composite Structures, *Vol. 29, No. 5 (2018) 623-633*
DOI: https://doi.org/10.12989/scs.2018.29.5.623

Curved-quartic-function elements with end-springs in series for direct analysis of steel frames

Si-Wei Liu [1a], Jake Lok Yan Chan [2b], Rui Bai [*3] and Siu-Lai Chan [3c]

[1] *School of Civil Engineering, Sun-Yat-Sen University, China*
[2] *Department of Civil Engineering, The University of Hong Kong, Hong Kong, China*
[3] *Department of Civil and Environmental Engineering, The Hong Kong Polytechnic University, Hong Kong, China*

(*Received May 30, 2018, Revised November 9, 2018, Accepted November 19, 2018*)

Abstract. A robust element is essential for successful design of steel frames with Direct analysis (DA) method. To this end, an innovative and efficient curved-quartic-function (CQF) beam-column element using the fourth-order polynomial shape function with end-springs in series is proposed for practical applications of DA. The member initial imperfection is explicitly integrated into the element formulation, and, therefore, the *P-δ* effect can be directly captured in the analysis. The series of zero-length springs are placed at the element ends to model the effects of semi-rigid joints and material yielding. One-element-per-member model is adopted for design bringing considerable savings in computer expense. The incremental secant stiffness method allowing for large deflections is used to describe the kinematic motion. Finally, several problems are studied in this paper for examining and validating the accuracy of the present formulations. The proposed element is believed to make DA simpler to use than existing elements, which is essential for its successful and widespread adoption by engineers.

Keywords: second-order; steel; imperfection; semi-rigid; design; plastic hinge

1. Introduction

Direct analysis (DA) is the new and codified approach to the design of steel structures. The vital factors, e.g., initial imperfections, residual stress, flexible joints, material yielding, etc., relating to the stability are comprehensively considered in a direct and simple manner. This method has become the preferred design method for steel structures as recommended in the modern design codes, such as Eurocode 3 (2005), CoPSC (2011) and ANSI/AISC360-16 (2016) and so on.

The basic difference between DA and the conventional effective length method is that DA checks and designs structures and members by directly inspecting the member internal forces with the explicitly modeling of imperfections. Naturally, reliable and robust beam-column elements and numerical incremental-iterative schemes are essential for successful implementation of DA to practical design.

In the past decades, some researchers proposed several sophisticated elements for the use of DA. For examples, Liew *et al*. (1993a, b) proposed an efficient element using refined plastic hinge method for inelastic analysis of steel members. Chan and Zhou (1994, 1995) formulated an advanced element with the 5th-order shape function and initial imperfections for the robust second-order design of members. Later, Gu and Chan (2005) developed an initially curved stability-function element for simulating ultra-slender members under large axial loads. Recently, Liu *et al*. (2014a, b) proposed a beam-column element with an arbitrarily-located hinge aiming for capturing the inelastic behaviors of members.

Imperfections existing in structures affect the stability and strength of the system and member. The effects of the initial imperfections must be considered in a successful design according to Chan and Zhou (1994), Iu (2016a), Cai *et al*. (2017), Gao *et al*. (2017) and Yang *et al*. (2018). To efficiently model the member initial out-of-plumbness, the one-element-per-member model is recommended by Liu *et al*. (2014a, b), who claim it is necessary for practical uses of DA. The beam-column element should be capable of simulating a member with only one element in geometrically nonlinear problems. Therefore, a new beam-column element with the quartic shape function and the initial curve is proposed in this paper for robust and efficient use of DA for practical design.

Joint rigidity significantly affects member deformation, structural deflection, and force distribution, as reported by Bayat and Zahrai (2016), Artar and Daloglu (2015) Torbaghan (Torbaghan *et al*. 2018) and Zohra (Zohra and Abd Nacer 2018). In the conventional design, the member connections are ideally assumed to be perfectly rigid or pinned for simplicity in the analysis, and the tedious detailing work on joints is required to satisfy these assumptions. Under the concept of DA, the member end's flexible behaviors should be directly modeled in the analysis to reflect the actual structural response. Zero-length

*Corresponding author, Research Associate,
E-mail: rui.bai@connect.polyu.hk
[a] Associate Professor, E-mail: siwei.liu@connect.polyu.hk
[b] Ph.D. Student, E-mail: jakechan@jakechan.com
[c] Chair Professor, E-mail: ceslchan@polyu.edu.hk

ISSN: 1229-9367 (Print), 1598-6233 (Online)

connection elements are added to the element ends to model semi-rigid joints in the present study. This is the most effective integration method extensively adopted by researchers, such as Liew *et al*. (1993a, b, 2000), Chan and Zhou (1994), Kim and Choi (2001), Chiorean (2009 and 2017), Thai and Kim (2015) and Nguyen and Kim (2013, 2016).

Material yielding affects the member deflection and overall stability of a frame (Zhang *et al*. 2014, 2016, Saritas and Koseoglu 2015, White *et al*. 2016, Ziemian and Abreu 2018), which should be properly reflected in the DA. In this paper, the lumped plasticity model is introduced for an efficient simulation. Dimensionless springs are inserted at the element ends to reflect the sectional plasticity in a concentrated manner, which is treated as the practical solution for the inelastic design of steel frames as reported by Liu *et al*. (2014a). Several researchers have adopted this algorithm for their studies, such as King *et al*. (1992), White (1993), Liew *et al*. (1993a, b), Iu (2016b), Hoang *et al*. (2015), Lezgy-Nazargah (Lezgy-Nazargah and Kafi 2015), Thai *et al*. (2017), Alhasawi *et al*. (2017) and Farahi and Erfani (2017) and so on. Therefore, effects of material yielding and semi-rigid joints are simulated by pseudo-springs. To combine their effects, the zero-length springs elements are linked together to form a springs-in-series model as proposed by Yau and Chan (1994), which is employed in the present study.

In this paper, the derivations on element secant relations and tangent stiffness matrixes are detailed. To consider joints semi-rigid behavior and the lumped plasticity, the zero-length pseudo-spring elements are incorporating into the proposed element formulations. A springs-in-series model is introduced to combine the effects of semi-rigid joints and material yielding. The incremental secant stiffness method is employed to facilitate the moderately large deflections during the numerical procedure. At the end of this paper, several benchmarking examples are employed for the validation and verification of the proposed beam-column element formulations.

2. Assumptions

In the element derivations, small strains are assumed and, however, deflections can be moderately large. The Euler-Bernoulli hypothesis is employed to assume the strain remains plane and linearly distributed across the section. The internal DOFs in the element formulations are used for capturing the *P-δ* deformations, and the loads are only applied to the external nodes. Semi-rigid joints are modelled by zero-length springs of equivalent stiffness. Material yielding along the member is concentrated at the element ends, and simulated by plastic hinge springs. Shear and warping deformations are ignored.

3. Element formulations

3.1 Imperfect single columns with idealized boundary conditions

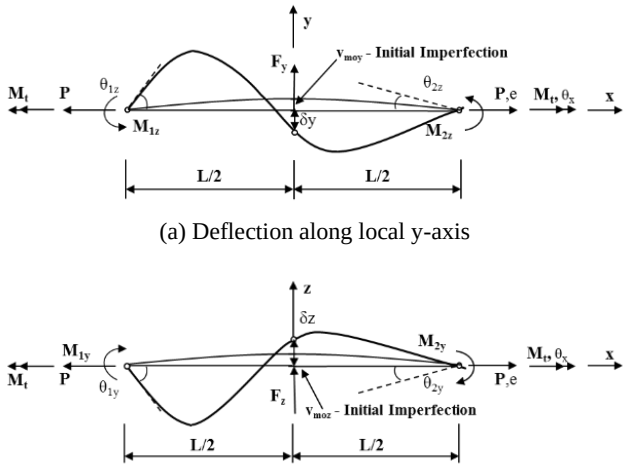

(a) Deflection along local y-axis

(b) Deflection along local z-axis

Fig. 1 Forces vs. deflections of the quartic-function element

A parabolic equation is assumed for the member imperfection as

$$\begin{aligned} v_{0y}(x) &= v_{m0y}\left[1-(2x/L)\right] \\ v_{0z}(x) &= v_{m0z}\left[1-(2x/L)\right] \end{aligned} \tag{1}$$

in which v_{m0y} and v_{m0z} are the magnitudes of the imperfections at the middle of the element.

The lateral deflection v of the element is assumed to be the quartic shape function as below

$$v(x) = a_0 + a_1 x + a_2 x^2 + a_3 x^3 + a_4 x^4 \tag{2}$$

where, a_0 to a_4 is the coefficients in the shape function.

Boundary conditions are applied to the quartic shape function, as indicated in Fig. 1, which are given as

$$when \quad x = -\frac{1}{2}L \quad v = 0 \quad \frac{dv}{dx} = \theta_1 \tag{1}$$

$$when \quad x = +\frac{1}{2}L \quad v = 0 \quad \frac{dv}{dx} = \theta_2 \tag{1}$$

$$when \quad x = 0 \quad v = \delta \tag{1}$$

in which, L is the element length; θ_1 & θ_2 are the rotational angles at the ends; and δ is the deflection at the mid-span, which is the internal degree-of-freedom aiming to simulate the *P-δ* effect only.

By solving the above boundary conditions, the shape function can be rewritten as

$$v(x) = \{N\}\{u\}^T \tag{6}$$

where, $\{N\}$ is the vector of parameters in the shape function for the lateral deformations, where the parameters; and $\{u\}$ is the vector of DOFs. They are expressing as

$$\{N\}^T=\left\{\begin{array}{c}-\dfrac{(L-2x)^2x(L+2x)}{4L^3}\\ \dfrac{\left(L^2-4x^2\right)^2}{L^4}\\ -\dfrac{(L-2x)x(L+2x)^2}{4L^3}\end{array}\right\} \tag{7}$$

$$\{u\}=\{\theta_1 \quad \delta \quad \theta_2\} \tag{8}$$

For the spatial analysis, the element shape functions at the two principle axes can be given as

$$\begin{aligned} v_y(x)&=\{N\}\{\theta_{1y} \quad \delta_z \quad \theta_{2y}\}^T\\ v_z(x)&=\{N\}\{\theta_{1z} \quad \delta_y \quad \theta_{2z}\}^T\end{aligned} \tag{9}$$

The shape functions for axial and torsional deformations are assumed to be linearly interpolated.

$$\begin{aligned} \mathrm{u}(\mathrm{x})&=e\left(\frac{1}{2}+\frac{x}{L}\right)\\ \mathrm{t}(\mathrm{x})&=\theta_t\left(\frac{1}{2}+\frac{x}{L}\right)\end{aligned} \tag{10}$$

where, e and θ_t are the axial and torsional deformations along with the member, respectively.

3.2 Bowing effects

The member bowing due to deformations of the lateral deflections are derived as

$$\begin{aligned} u_b&=\frac{1}{2}\int_L\left(\dot{v}_y^{\,2}+2\dot{v}_{0y}\dot{v}_y\right)\mathrm{dx}+\frac{1}{2}\int_L\left(\dot{v}_z^{\,2}+2\dot{v}_{0z}\dot{v}_z\right)\mathrm{dx}\\ &=\frac{2\mathrm{v}_{\mathrm{m0y}}\left[32\delta_z+L\left(\theta_{1y}-\theta_{2y}\right)\right]}{15L}+\frac{2\mathrm{v}_{\mathrm{m0z}}\left[32\delta_y+L\left(\theta_{1z}-\theta_{2z}\right)\right]}{15L}\\ &+\frac{512\delta_z^{\,2}-16L\delta_z\left(\theta_{1y}-\theta_{2y}\right)+L^2\left(8\theta_{1y}^{\,2}+5\theta_{1y}\theta_{2y}+8\theta_{2y}^{\,2}\right)}{210L}\\ &+\frac{512\delta_y^{\,2}-16L\delta_y\left(\theta_{1z}-\theta_{2z}\right)+L^2\left(8\theta_{1z}^{\,2}+5\theta_{1z}\theta_{2z}+8\theta_{2z}^{\,2}\right)}{210L}\end{aligned} \tag{11}$$

3.3 Potential energy function

Shear strain energy is purposely ignored and the total potential energy can be generated and given as

$$\begin{aligned} U&=\frac{1}{2}\int_L EA\dot{u}^2dx+\frac{1}{2}\int_L EI_y\ddot{v}_y^{\,2}dx+\frac{1}{2}\int_L EI_z\ddot{v}_z^{\,2}dx+\frac{1}{2}\int_L GJ\dot{t}^2dx\\ &+\frac{1}{2}\int_L P\left(\dot{v}_y^{\,2}+2\dot{v}_{0y}\dot{v}_y\right)dx+\frac{1}{2}\int_L P\left(\dot{v}_z^{\,2}+2\dot{v}_{0z}\dot{v}_z\right)dx\end{aligned} \tag{12}$$

where, EA is the axial rigidity; EI_y and EI_z are the bending stiffness about two principle axes; GJ is the rigidity in torsion.

3.4 Secant relations

The equilibrium conditions are established and computed as

$$\begin{aligned} P&=\frac{e}{L}EA+\frac{64}{15L^2}EAv_{m0z}\delta_y+\frac{256}{105L^2}EA\delta_y^{\,2}\\ &+\frac{64}{15L^2}EAv_{m0y}\delta_z+\frac{256}{105L^2}EA\delta_z^{\,2}\\ &+\frac{4}{105}EA\theta_{1y}^{\,2}+\frac{4}{105}EA\theta_{1z}^{\,2}+\frac{4}{105}EA\theta_{2y}^{\,2}\\ &+\left(-\frac{2}{15L}EAv_{m0y}+\frac{8}{105L}EA\delta_z\right)\theta_{2y}\\ &+\left(\frac{2}{15L}EAv_{m0y}-\frac{8}{105L}EA\delta_z+\frac{1}{42}EA\theta_{2y}\right)\theta_{1y}\\ &+(-\frac{2}{15L}EAv_{m0z}+\frac{8}{105L}EA\delta_y)\theta_{2z}+\frac{4}{105}EA\theta_{2z}^{\,2}\\ &+\left(\frac{2}{15L}EAv_{m0z}-\frac{8}{105L}EA\delta_y+\frac{1}{42}EA\theta_{2z}\right)\theta_{1z}\end{aligned} \tag{13}$$

$$\begin{aligned} M_{1y}&=\frac{36}{5L}EI_y\theta_{1y}-\frac{128}{5L^2}EI_y\delta_z-\frac{6}{5L}EI_y\theta_{2y}\\ &+\frac{8}{105}LP\theta_{1y}-\frac{8}{105}P\delta_z+\frac{1}{42}LP\theta_{2y}+\frac{2}{15}Pv_{m0y}\end{aligned} \tag{14}$$

$$\begin{aligned} M_{1z}&=-\frac{128}{5L^2}EI_z\delta_y+\frac{36}{5L}EI_z\theta_{1z}-\frac{6}{5L}EI_z\theta_{2z}\\ &-\frac{8}{105}P\delta_y+\frac{8}{105}LP\theta_{1z}+\frac{1}{42}LP\theta_{2z}+\frac{2}{15}Pv_{m0z}\end{aligned} \tag{15}$$

$$\begin{aligned} F_z&=-\frac{128}{5L^2}EI_y\theta_{1y}+\frac{128}{5L^2}EI_y\theta_{2y}+\frac{1024}{5L^3}EI_y\delta_z\\ &-\frac{8P}{105}\theta_{1y}+\frac{8}{105}P\theta_{2y}+\frac{512}{105L}P\delta_z+\frac{64}{15L}Pv_{m0y}\end{aligned} \tag{16}$$

$$\begin{aligned} F_y&=\frac{1024}{5L^3}EI_z\delta_y-\frac{128}{5L^2}EI_z\theta_{1z}+\frac{128}{5L^2}EI_z\theta_{2z}\\ &+\frac{512}{105L}P\delta_y-\frac{8}{105}P\theta_{1z}+\frac{8}{105}P\theta_{2z}+\frac{64}{15L}Pv_{m0z}\end{aligned} \tag{17}$$

$$\begin{aligned} M_{2y}&=-\frac{6}{5L}EI_y\theta_{1y}+\frac{36}{5L}EI_y\theta_{2y}+\frac{128}{5L^2}EI_y\delta_z\\ &+\frac{1}{42}LP\theta_{1y}+\frac{8}{105}LP\theta_{2y}+\frac{8}{105}P\delta_z-\frac{2}{15}Pv_{m0y}\end{aligned} \tag{18}$$

$$\begin{aligned} M_{2z}&=\frac{128}{5L^2}EI_z\delta_y-\frac{6}{5L}EI_z\theta_{1z}+\frac{36}{5L}EI_z\theta_{2z}\\ &+\frac{8}{105}P\delta_y+\frac{1}{42}LP\theta_{1z}+\frac{8}{105}LP\theta_{2z}-\frac{2}{15}Pv_{m0z}\end{aligned} \tag{19}$$

$$M_t=\frac{GJ\theta_x}{L} \tag{20}$$

3.5 Tangent stiffness matrixes

Tangent stiffness matrixes are calculated by the second variation of the Eq. (12) for predicting the increased displacement to an applied force vector in the incremental-iterative numerical procedure.

$$\delta^2\Pi=\frac{\partial^2\Pi}{\partial u_i\partial u_j}\delta u_i\delta u_j=\left[\frac{\partial F_i}{\partial u_j}+\frac{\partial f_i}{\partial P}\frac{\partial P}{\partial u_j}\right]\delta u_i\delta u_j \tag{21}$$

where, i, j are taken from 1 to 8; f_i is the force vector; u_i is the displacement vector. Re-arranging, the tangent stiffness of the element is re-written as

$$[k]_e=[k]_L+[k]_G \tag{22}$$

where, $[k]_L$ is the linear elastic stiffness matrix; and $[k]_G$ is the geometric matrix for considering second-order effects. They are expressed as

$$[k]_L=\begin{bmatrix}
\frac{EA}{L} & 0 & 0 & 0 & 0 & 0 & 0 & 0\\
 & \frac{36EIy}{5L} & 0 & 0 & -\frac{128EIy}{5L^2} & 0 & -\frac{6EIy}{5L} & 0\\
 & & \frac{36EIz}{5L} & 0 & 0 & -\frac{128EIz}{5L^2} & 0 & -\frac{6EIz}{5L}\\
 & & & 0 & 0 & 0 & 0 & 0\\
 & S. & & & \frac{1024EIy}{5L^3} & 0 & \frac{128EIy}{5L^2} & 0\\
 & & Y. & & & \frac{1024EIz}{5L^3} & 0 & \frac{128EIz}{5L^2}\\
 & & & M. & & & \frac{36EIy}{5L} & 0\\
 & & & & & & & \frac{36EIz}{5L}
\end{bmatrix} \tag{23}$$

$$[k]_G=\begin{bmatrix}
0 & k_{G1,2} & k_{G1,3} & 0 & k_{G1,5} & k_{G1,6} & k_{G1,7} & k_{G1,8}\\
 & k_{G2,2} & k_{G2,3} & 0 & k_{G2,5} & k_{G2,6} & k_{G2,7} & k_{G2,8}\\
 & & k_{G3,3} & 0 & k_{G3,5} & k_{G3,6} & k_{G3,7} & k_{G3,8}\\
 & & & 0 & 0 & 0 & 0 & 0\\
 & S. & & & k_{G5,5} & k_{G5,6} & k_{G5,7} & k_{G5,8}\\
 & & Y. & & & k_{G6,6} & k_{G6,7} & k_{G6,8}\\
 & & & M. & & & k_{G7,7} & k_{G7,8}\\
 & & & & & & & k_{G8,8}
\end{bmatrix} \tag{24}$$

in which, the expressions for the factors in $[k]_G$ are given as

$$k_{G1,2}=\frac{2}{15L}EAv_{m0y}-\frac{8}{105L}EA\delta_z+\frac{8}{105}EA\theta_{1y}+\frac{1}{42}EA\theta_{2y} \tag{25}$$

$$k_{G2,2}=\frac{8LP}{105}+\frac{EA\left(28v_{m0y}-16\delta_z+16L\theta_{1y}+5L\theta_{2y}\right)^2}{44100L} \tag{26}$$

$$k_{G1,3}=\frac{2}{15L}EAv_{m0z}-\frac{8}{105L}EA\delta_y+\frac{8}{105}EA\theta_{1z}+\frac{1}{42}EA\theta_{2z} \tag{27}$$

$$k_{G2,3}=\frac{EA\left(28v_{m0y}-16\delta_z+16L\theta_{1y}+5L\theta_{2y}\right)}{44100L}*\left(28v_{m0z}-16\delta_y+16L\theta_{1z}+5L\theta_{2z}\right) \tag{28}$$

$$k_{G3,3}=\frac{8}{105}LP+\frac{EA\left(28v_{m0z}-16\delta_y+16L\theta_{1z}+5L\theta_{2z}\right)^2}{44100L} \tag{29}$$

$$k_{G1,5}=\frac{64}{15L^2}EAv_{m0y}+\frac{512}{105L^2}EA\delta_z-\frac{8}{105L}EA\theta_{1y}+\frac{8}{105L}EA\theta_{2y} \tag{30}$$

$$k_{G2,5}=\frac{4EA\left(28v_{m0y}-16\delta_z+16L\theta_{1y}+5L\theta_{2y}\right)}{11025L^2}*\left[56v_{m0y}+64\delta_z+L\left(-\theta_{1y}+\theta_{2y}\right)\right]-\frac{8P}{105} \tag{31}$$

$$k_{G3,5}=\frac{4EA\left[56v_{m0y}+64\delta_z+L\left(-\theta_{1y}+\theta_{2y}\right)\right]}{11025L^2}*\left(28v_{m0z}-16\delta_y+16L\theta_{1y}+5L\theta_{2z}\right) \tag{32}$$

$$k_{G5,5}=\frac{512P}{105L}+\frac{64EA\left[56v_{m0y}+64\delta_z+L\left(-\theta_{1y}+\theta_{2y}\right)\right]^2}{11025L^3} \tag{33}$$

$$k_{G1,6}=\frac{64}{15L^2}EAv_{m0z}+\frac{512}{105L^2}EA\delta_y-\frac{8}{105L}EA\theta_{1z}+\frac{8}{105L}EA\theta_{2z} \tag{34}$$

$$k_{G2,6}=\frac{4EA\left(28v_{m0y}-16\delta_z+16L\theta_{1y}+5L\theta_{2y}\right)}{11025L^2}*\left[56v_{m0z}+64\delta_y+L\left(-\theta_{1z}+\theta_{2z}\right)\right] \tag{35}$$

$$k_{G3,6}=\frac{4EA\left(28v_{m0z}-16\delta_y+16L\theta_{1z}+5L\theta_{2z}\right)}{11025L^2}*\left[56v_{m0z}+64\delta_y+L\left(-\theta_{1z}+\theta_{2z}\right)\right]-\frac{8P}{105} \tag{36}$$

$$k_{G5,6}=\frac{64EA\left[56v_{m0y}+64\delta_z+L\left(-\theta_{1y}+\theta_{2y}\right)\right]}{11025L^3}*\left[56v_{m0z}+64\delta_y+L\left(-\theta_{1z}+\theta_{2z}\right)\right] \tag{37}$$

$$k_{G6,6}=\frac{64EA\left(56v_{m0z}+64\delta_y+L\left(-\theta_{1z}+\theta_{2z}\right)\right)^2}{11025L^3} \tag{38}$$

$$+\frac{512P}{105L} \tag{38}$$

$$k_{G1,7}=-\frac{2}{15L}EAv_{m0y}+\frac{8}{105L}EA\delta_z +\frac{1}{42}EA\theta_{1y}+\frac{8}{105}EA\theta_{2y} \tag{39}$$

$$k_{G2,7}=\frac{LP}{42}+\frac{EA\left(28v_{m0y}-16\delta_z+16L\theta_{1y}+5L\theta_{2y}\right)}{44100L} *\left(-28v_{m0y}+16\delta_z+5L\theta_{1y}+16L\theta_{2y}\right) \tag{40}$$

$$k_{G3,7}=\frac{EA\left(-28v_{m0y}+16\delta_z+5L\theta_{1y}+16L\theta_{2y}\right)}{44100L} *\left(28v_{m0z}-16\delta_y+16L\theta_{1z}+5L\theta_{2z}\right) \tag{41}$$

$$k_{G5,7}=\frac{8P}{105}-\frac{4EA\left[-56v_{m0y}-64\delta_z+L\left(-\theta_{1y}+\theta_{2y}\right)\right]}{11025L^2} *\left(-28v_{m0y}+16\delta_z+5L\theta_{1y}+16L\theta_{2y}\right) \tag{42}$$

$$k_{G6,7}=-\frac{4EA\left(-28v_{m0y}+16\delta_z+5L\theta_{1y}+16L\theta_{2y}\right)}{11025L^2} *\left[-56v_{m0z}-64\delta_y+L\left(-\theta_{1z}+\theta_{2z}\right)\right] \tag{43}$$

$$k_{G7,7}=\frac{8LP}{105}+\frac{EA\left(-28v_{m0y}+16\delta_z+5L\theta_{1y}+16L\theta_{2y}\right)^2}{44100L} \tag{44}$$

$$k_{G1,8}=-\frac{2}{15L}EAv_{m0z}+\frac{8}{105L}EA\delta_y +\frac{1}{42}EA\theta_{1z}+\frac{8}{105}EA\theta_{2z} \tag{45}$$

$$k_{G2,8}=\frac{EA\left(28v_{m0y}-16\delta_z+16L\theta_{1y}+5L\theta_{2y}\right)}{44100L} *\left(-28v_{m0z}+16\delta_y+5L\theta_{1z}+16L\theta_{2z}\right) \tag{46}$$

$$k_{G3,8}=\frac{LP}{42}+\frac{EA\left(28v_{m0z}-16\delta_y+16L\theta_{1z}+5L\theta_{2z}\right)}{44100L} *\left(-28v_{m0z}+16\delta_y+5L\theta_{1z}+16L\theta_{2z}\right) \tag{47}$$

$$k_{G5,8}=\frac{4EA\left[56v_{m0y}+64\delta_z+L\left(-\theta_{1y}+\theta_{2y}\right)\right]}{11025L^2} *\left(-28v_{m0z}+16\delta_y+5L\theta_{1z}+16L\theta_{2z}\right) \tag{48}$$

$$k_{G6,8}=\frac{8P}{105}-\frac{4EA\left(-28v_{m0z}+16\delta_y+5L\theta_{1z}+16L\theta_{2z}\right)}{11025L^2} *\left[-56v_{m0z}-64\delta_y+L\left(\theta_{1z}-\theta_{2z}\right)\right] \tag{49}$$

$$k_{G7,8}=\frac{EA\left(-28v_{m0y}+16\delta_z+5L\theta_{1y}+16L\theta_{2y}\right)}{44100L} *\left(-28v_{m0z}+16\delta_y+5L\theta_{1z}+16L\theta_{2z}\right) \tag{50}$$

$$k_{G8,8}=\frac{8LP}{105}+\frac{EA\left(-28v_{m0z}+16\delta_y+5L\theta_{1z}+16L\theta_{2z}\right)^2}{44100L} \tag{51}$$

3.6 Static condensation algorithm for stiffness matrix

To be compatible for the conventional computer program using the cubic Hermite elements and for computational efficiency, the internal DOFs of the proposed element are condensed by the static condensation algorithm. The DOFs and the corresponding forces can be expressed as

$$\{u_i\}=\begin{Bmatrix}\delta_z & \delta_y\end{Bmatrix}^T \tag{52}$$

$$\{u_e\}=\begin{Bmatrix}e & \theta_{11y} & \theta_{11z} & \theta_x & \theta_{22y} & \theta_{22z}\end{Bmatrix}^T \tag{53}$$

$$\{f\}=\begin{Bmatrix}P & M_{11y} & M_{11z} & M_x & M_{22y} & M_{22z}\end{Bmatrix}^T \tag{54}$$

Herein, $[k]^*$ is the condensed stiffness matrix and $\{f\}$ is the force vector at the external nodes, and they are given as

$$[k]^*\{u_e\}=\{f\} \tag{55}$$

where

$$[k]^*=[k]_{ee}-[k]_{ie}^T[k]_{ii}^{-1}[k]_{ie} \tag{56}$$

in which, $[k]_{ee}$ and $[k]_{ii}$ are the stiffness matrixes at the external and internal nodes, respectively; and $[k]_{ie}$ is the correlated stiffness matrixes between the external and internal nodes.

To reduce the computational expense on matrix inverse, the $[k]_{ii}^{-1}$ is derived and given as below

$$[k_{ii}]^{-1}=\frac{1}{\alpha}\begin{bmatrix}\beta_1 & \beta_2\\ \beta_3 & \beta_4\end{bmatrix} \tag{57}$$

where

$$\beta_1=11025L^3\begin{pmatrix}35280EI_z+840L^2P\\ +EA\left(56v_{m0z}+64\delta_y+L(-\theta_{1z}+\theta_{2z})\right)^2\end{pmatrix} \tag{58}$$

$$\beta_2 = 11025EAL^3(56v_{m0y} + 64\delta_z + L(-\theta_{1y} + \theta_{2y})) \\ *(56v_{m0z} + 64\delta_y + L(-\theta_{1z} + \theta_{2z})) \quad (59)$$

$$\beta_3 = 11025EAL^3(56v_{m0y} + 64\delta_z + L(-\theta_{1y} + \theta_{2y})) \\ (-56v_{m0z} - 64\delta_y + L(\theta_{1z} - \theta_{2z})) \quad (60)$$

$$\beta_4 = 11025L^3\begin{pmatrix} 35280EI_y + 840L^2P \\ +EA(56v_{m0y} + 64\delta_z + L(-\theta_{1y} + \theta_{2y}))^2 \end{pmatrix} \quad (61)$$

$$\alpha = 64(-EA^2c_1c_2 + (b_1 + EAc_1)(b_2 + EAc_2)) \quad (6)$$

in which

$$b_1 = 35280EI_y + 840L^2P \quad (63)$$

$$b_2 = 35280EI_z + 840L^2P \quad (64)$$

$$c_1 = (56v_{m0y} + 64\delta_z + L(-\theta_{1y} + \theta_{2y}))^2 \quad (65)$$

$$c_2 = (56v_{m0z} + 64\delta_y + L(-\theta_{1z} + \theta_{2z}))^2 \quad (66)$$

4. Spring-in-series model

To consider the effects of semi-rigid joint and material yielding, two types of pseudo-springs are introduced as indicated in Fig. 2, e.g., connection and section springs. The flexible joints at member ends are simulated by the connection spring, while the inelastic behavior of the member is considered by the section spring. To integrate the stiffness of these springs, the zero-length springs elements (Yau and Chan 1994) are linked to form a springs-in-series model is employed in the present study. The combined hinge stiffness can be computed as

$$S = \frac{S_C S_S}{S_C + S_S} \quad (67)$$

in which, S is the combined hinge stiffness at the element ends; S_C denotes for stiffness of the semi-rigid joint; and S_S is the stiffness of the plastic hinge.

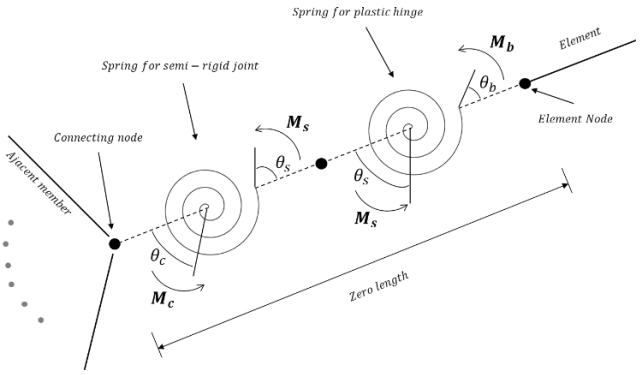

Fig. 2 Springs-in-series model

4.1 Incorporation of end-springs

To incorporate the combined end spring to the element matrices, the procedure proposed by (Liu *et al*. 2014a) is introduced. The condensed stiffness matrix of an element is generated as

$$[k^*] = \begin{bmatrix} k11^* & k12^* & k13^* & k14^* & k15^* & k16^* \\ & k22^* & k23^* & k24^* & k25^* & k26^* \\ S. & & k33^* & k34^* & k35^* & k36^* \\ & Y. & & k44^* & k45^* & k46^* \\ & & M. & & k55^* & k56^* \\ & & & & & k66^* \end{bmatrix} \quad (68)$$

To incorporate the rotational springs to the stiffness matrix, the condensed stiffness matrix is updated to $[\tilde{k}]$ and given as below

$$[\tilde{k}] = \begin{bmatrix} k11^* & k12^* & k13^* & k14^* & k15^* & k16^* \\ & \tilde{k}22 & k23^* & k24^* & \tilde{k}25 & k26^* \\ S. & & \tilde{k}33 & k34^* & k35^* & \tilde{k}36 \\ & Y. & & k44^* & k45^* & k46^* \\ & & M. & & \tilde{k}55 & k56^* \\ & & & & & \tilde{k}66 \end{bmatrix} \quad (69)$$

where

$$\tilde{k}22 = S_{Ly} - \frac{S_{Ly}^2\left(k55^* + S_{Ry}\right)}{\left(k22^* + S_{Ly}\right)\left(k55^* + S_{Ry}\right)} \quad (70)$$

$$\tilde{k}25 = \frac{S_{Ly}S_{Ry}k25^*}{\left(k22^* + S_{Ly}\right)\left(k55^* + S_{Ry}\right) - k25^*k52^*} \quad (71)$$

$$\tilde{k}55 = S_{Ry} - \frac{S_{Ry}^2\left(k22^* + S_{Ly}\right)}{\left(k22^* + S_{Ly}\right)\left(k55^* + S_{Ry}\right) - k25^*k52^*} \quad (72)$$

$$\tilde{k}33 = S_{Lz} - \frac{S_{Lz}^2\left(k66^* + S_{Rz}\right)}{\left(k33^* + S_{Lz}\right)\left(k66^* + S_{Rz}\right) - k36^*k63^*} \quad (73)$$

$$\tilde{k}36 = \frac{S_{Lz}S_{Rz}k36^*}{\left(k33^* + S_{Lz}\right)\left(k66^* + S_{Rz}\right) - k36^*k63^*} \quad (74)$$

$$\tilde{k}66 = S_{Rz} - \frac{S_{Rz}^2\left(k33^* + S_{Lz}\right)}{\left(k33^* + S_{Lz}\right)\left(k66^* + S_{Rz}\right) - k36^*k63^*} \quad (75)$$

in which, S_{Ly}, S_{Ry}, S_{Lz} and S_{Rz} are the combined hinge stiffness at the left and right ends, respectively.

The rotations at the element ends can be computed by

$$\begin{Bmatrix} \Delta\theta_{11y} \\ \Delta\theta_{22y} \end{Bmatrix} = \begin{bmatrix} k22^* + S_{Ly} & k25^* \\ k52^* & k55^* + S_{Ry} \end{bmatrix}^{-1} \begin{bmatrix} S_{Ly} & 0 \\ 0 & S_{Ry} \end{bmatrix} \begin{Bmatrix} \Delta\theta_{s1y} \\ \Delta\theta_{s2y} \end{Bmatrix} \quad (76)$$

$$\begin{Bmatrix}\Delta\theta_{11z}\\ \Delta\theta_{22z}\end{Bmatrix}=\begin{bmatrix}k33^{*}+S_{Lz} & k36^{*}\\ k63^{*} & k66^{*}+S_{Rz}\end{bmatrix}^{-1}\begin{bmatrix}S_{Lz} & 0\\ 0 & S_{Rz}\end{bmatrix}\begin{Bmatrix}\Delta\theta_{s1z}\\ \Delta\theta_{s2z}\end{Bmatrix} \quad (77)$$

where, $\Delta\theta_{1y}$, $\Delta\theta_{1z}$, $\Delta\theta_{2y}$, and $\Delta\theta_{2z}$ are the incremental rotations at the beam-column element; and $\Delta\theta_{c1y}$, $\Delta\theta_{c1z}$, $\Delta\theta_{c2y}$, and $\Delta\theta_{c2z}$ are the incremental rotations at the external nodes.

4.2 Semi-rigid joint model

Extensive numerical and experimental research has been conducted to investigate the nonlinear behaviors of the semi-rigid joints in the last two decades. For example, Chen and his associates proposed a series of studied on semi-rigid joints, e.g., the references (Lui and Chen 1987, Chen and Kishi 1989, Abdalla and Chen 1995 and Kishi *et al*. 1996). The semi-rigid behavior is usually described by the moment versus joint rotation relations, while the joint stiffness changes according to the applied moments. Therefore, the instantaneous rotational stiffness of a semi-rigid joint can be calculated as

$$S_c^i=\frac{dM_c}{d\theta_s^i} \quad (78)$$

in which, $S_c{}^i$ is the instantaneous stiffness of the semi-rigid joint; Mc is the current moment applied at the joint; and $\theta_s{}^i$ is the current rotation of the semi-rigid joint at the i^{th} iteration.

In the conventional practice, the Kishi-Chen (Chen and Kishi 1989) model is widely adopted because of its support by extensive experimental results. This model is given in the following

$$M=\frac{S_0\left|\theta_s\right|}{\left[1+\left|\theta_s/\theta_p\right|^n\right]^{1/n}} \quad (79)$$

where, S_0 is the initial stiffness of the joint; θ_p is the plastic rotation; and n is the shape factor.

4.3 Plastic hinge model

The numerical simulation technique using the plastic hinge model is employed for the practical utilization of DA, which is considered to be the most efficient method for inelastic analysis of steel structures as reported by Liu *et al*. (2014a). The gradual plasticization of the critical sections is simulated by the section springs, whose stiffness is controlled by the forces applied at the hinge locations and mathematically expressed as below

$$S_S^i=10^{10}\frac{EI}{L} \quad when \quad M_a^i\le M_e\left(1-\left|P_a^i/P_c\right|\right) \quad (80)$$

$$S_S^i=\frac{EI}{L}\left[\frac{M_p\left(1-\left|P_a^i/P_c\right|\right)-M_a^i}{M_a^i-M_e\left(1-\left|P_a^i/P_c\right|\right)}\right] \quad (81)$$

$$when \quad M_e\left(1-\left|P_a^i/P_c\right|\right)<M_a^i<M_p\left(1-\left|P_a^i/P_c\right|\right)$$

$$S_S^i=10^{-10}\frac{EI}{L} \quad when \quad M_a^i\ge M_p\left(1-\left|P_a^i/P_c\right|\right) \quad (82)$$

in which, $M_a{}^i$ and $P_a{}^i$ are the current bending moment and the axial force applied at the hinge location, respectively; M_e, M_p and P_c is the elastic, plastic moments and axial capacities of a section, respectively.

5. Incremental secant stiffness model

To allow moderately large deflections and deformations in the analysis, the incremental secant stiffness method proposed by Chan (1992) is employed for the present study. The updated Lagrangian description is used, where the equilibrium condition is established referring to the last-know configuration, as indicated in Fig. 3.

Nevertheless, the rotations are updated in each iterative step and given as

$$\Delta\theta_{yi}=\Delta\kappa_{yi}+\Delta\mu_y \quad \text{where} \quad i=1\sim 2 \quad (83)$$

$$\Delta\theta_{zi}=\Delta\kappa_{zi}+\Delta\mu_z \quad \text{where} \quad i=1\sim 2 \quad (84)$$

where, $\Delta\kappa_{y1}$, $\Delta\kappa_{y2}$, $\Delta\kappa_{z1}$ and $\Delta\kappa_{z2}$ are the rotation increments at the last equilibrium condition; and $\Delta\mu_{yi}$ and $\Delta\mu_{zi}$ are the rigid body movements and calculated as

$$\Delta\beta_y=\frac{\Delta w_2-\Delta w_1}{L} \quad (85)$$

$$\Delta\beta_z=\frac{\Delta v_2-\Delta v_1}{L} \quad (86)$$

where, L_i is the member length at the last known configuration; Δw_1, Δw_2, Δv_1 and Δv_2 are the displacements

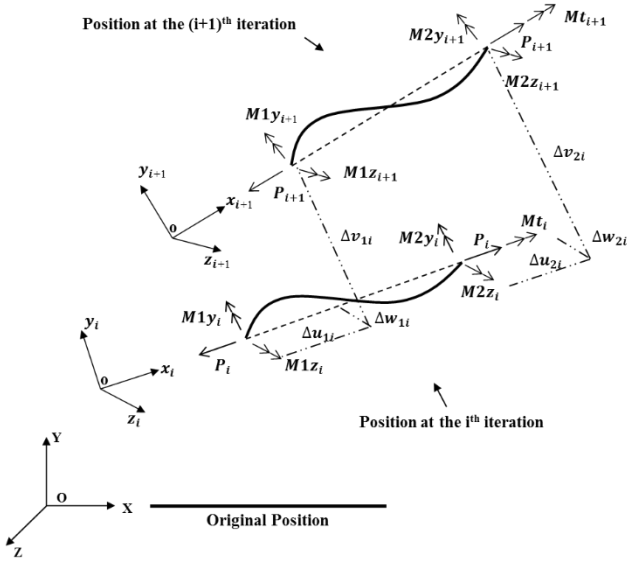

Fig. 3 Incremental kinematics of an element in three-dimensional space

at the last iteration.

The twist rotation can be calculated as

$$\Delta\theta_x = \Delta\theta_{x2} - \Delta\theta_{x1} \tag{87}$$

The axial displacement can be computed by

$$\Delta e = \Delta u_b - \Delta u_n \tag{88}$$

in which

$$\Delta u_n = L_{i+1} - L_i \tag{89}$$

and the Δu_b can be obtained by the first deviation of the expressions of u_b.

Consequentially, the corresponding nodal forces are calculated as

$$\{\Delta R\} = [K]_e \{\Delta u_i\} \tag{90}$$

$$\{R\}_{i+1} = \{R\}_i + \{\Delta R\} \tag{91}$$

where, $[K]_e$ denotes for the tangent stiffness matrix at the last iteration; and $\{R\}$ is the resisting force vector.

6. Verification examples

To examine and validate the proposed formulations, several famous and benchmarking examples are employed and analyzed. One-element per member model is adopted for the examples as follows.

6.1 Imperfect single columns with idealized boundary conditions

In this example, the performance of the new beam-column element is tested and compared with the benchmark solutions. Three slender steel columns with idealized boundary conditions, e.g., pinned-pinned, fixed-fixed and fixed-pinned, are analyzed. The initial member imperfection is assumed as L/500. These columns are made by rectangular hollow sections with 300 mm width, 300 height and 10 mm tube thickness. Yield strength and Young's modulus of elasticity are taken respectively as 355 MPa and 205000 MPa.

The stability function for the beam-column members is introduced for generating the benchmark results for comparisons, which can be expressed as follows for completeness.

$$\begin{aligned} y = &\frac{M_1}{P}\left[\frac{\sin(\kappa L - \kappa x)}{\sin kL} - \frac{L-x}{L}\right] - \\ &\frac{M_2}{P}\left[\frac{\sin \kappa L}{\sin \kappa L} - \frac{x}{L}\right] + \frac{\delta_0}{1 - P/\left(\pi^2 EI/L^2\right)} \sin\frac{\pi x}{L} \end{aligned} \tag{92}$$

where, κ denotes for $\sqrt{P/(EI)}$; and δ_0 is the magnitude of the imperfection at the mid-span.

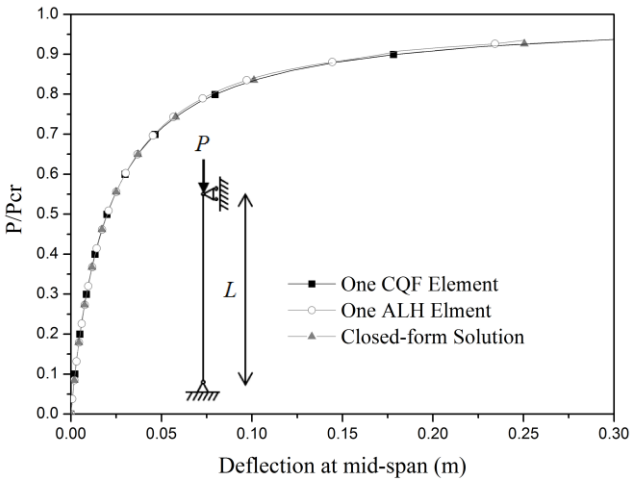

Fig. 4 Comparison analysis of the pined-pined column

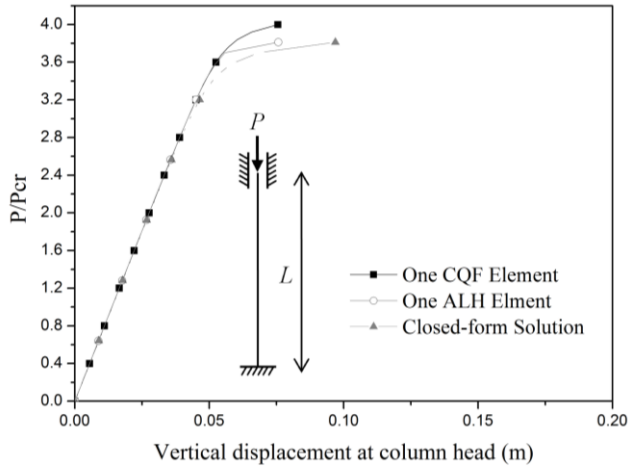

Fig. 5 Comparison analysis of the pined-fixed column

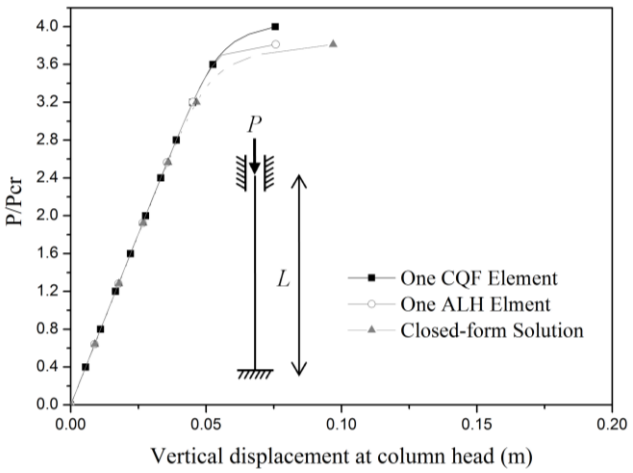

Fig. 6 Comparison analysis of the fixed-fixed column

The arbitrarily-located-hinge (ALH) element proposed by Liu *et al*. (2014a, b) is also employed for the comparison. The analysis results are presented from Fig. 4 to Fig. 6. From the comparisons, both the CQF and ALH elements can capture the nonlinear behaviors of the slender

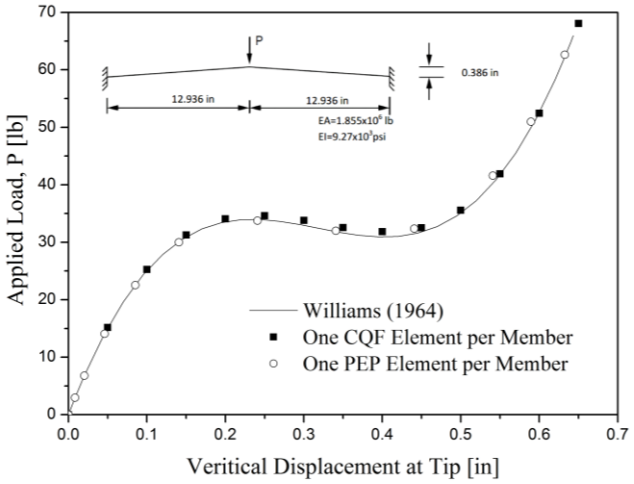

Fig. 7 Snap-through Analysis of William's toggle frame with rigid connections

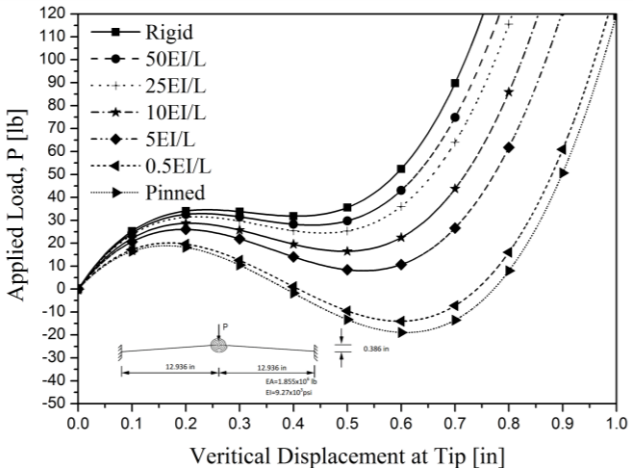

Fig. 8 Snap-through Analysis of William's toggle frame with semi-rigid connections

columns under high axial loads. The performances of the proposed element formulations are validated and proven to be accurate.

6.2 William's toggle frame

This example introduces the William's toggle frame to test the performance and efficiency of the proposed element, which has been extensively studied by researchers such as Zhou and Chan (1995) and Iu and Bradford (2012a, b) and so on. The toggle frame is formed by two members fixed at the end supports, where the overall span and height are 25.872 in and 0.386 in, respectively. The axial rigidity EA and flexural stiffness EI are 1.855×10^6 lb and 9.27×10^3 psi, respectively.

The PEP (Pointwise-Equilibrating-Polynomial) element proposed by Chan and Zhou (1994) is introduced for the comparisons. The comparison results are plotted in Fig. 7, where the results from Williams, PEP element and the proposed CQF element are presented and compared. It can be seen in this example that the nonlinear behavior of the

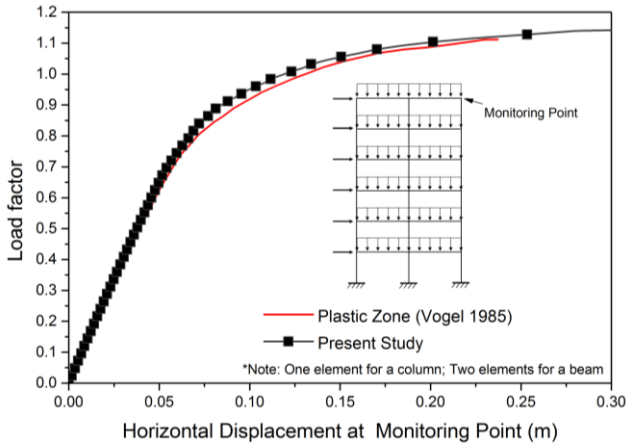

Fig. 9 Load vs. displacement curve of Vogel six-story frame

toggle frame can be captured well by the PEP and CQF elements. The predicted strength of CQF element is slightly higher than those reported by Williams during the snap-through stage. This example validates the proposed element formulations in handling highly nonlinear problems.

To evaluate the influence on the joint rigidity on the snap-thorough behaviors, the connection at the mid-span is assigned to be semi-rigid. The following cases of the stiffness for the joint are studied, e.g., rigid, 50EI/L, 25EI/L, 10EI/L, 5EI/L, 0.5EI/L and pinned. The analysis results are given in Fig. 8. It clearly indicates the connection rigidity significantly affects the behaviors of the toggle frame. In the Eurocode 3 (2005), when the joint stiffness is larger than 25EI/L or smaller than 0.5EI/L, it can be classified as rigid or pinned respectively. It can be seen the similar trend in Fig. 8, the load vs. displacement curves of the semi-rigid joint stiffness as 25EI/L and 50EI/L are closed to those analyzed by the rigid connection. The structural behaviors are closed to the pinned connection case, when the joint stiffness is equal to 0.5EI/L.

6.3 Vogel six-story frame

In this example, a six-story fame, originally analyzed by Vogel (1985) using plastic-zone approach as a benchmark solution, is introduced for validating the proposed element formulations in handling highly nonlinear behaviors composed of material yielding and large deflections. The material, geometric and section properties can be found in the literature by Liu *et al*. (2014a). For comparisons, the analysis results reported by Vogel (1985) are employed. The load vs. displacement results generated by the two numerical methods are plotted in Fig. 9. The predicted behaviors by both approaches are nearly identical, and the ultimate loads are closed. It can be concluded that the proposed element formulations are capable for simulating nonlinear inelastic behavior of a multi-story steel frame.

7. Conclusions

This paper proposes a curved quartic-function (CQF)

beam-column element with the fourth-order polynomial shape function for the design of steel structures by direct analysis (DA) approach. Initial member imperfection is explicitly simulated in the element formulation and therefore the *P-δ* effect can be directly captured in the analysis. One-element-per-member model is adopted for the frame design, bringing considerable savings in computer expense and data manipulating efforts for modeling. Series of zero-length springs are incorporated into the element ends to model the effects of semi-rigid joints and material yielding. The incremental secant stiffness method is employed for describing the kinematic motions to improve numerical efficiency. To reduce the difficulties in incorporating the new element into an existing nonlinear finite element program, the static condensation approach for the stiffness matrix is adopted with the internal degrees of freedom condensed. Finally, several benchmarking examples are presented to confirm the accuracy and reliability of the proposed element formulations. The proposed element formulations are contributory in making DA simple and reliable to use, which is essential for the successful introduction of DA to the profession.

Acknowledgments

The last author is grateful to the financial supports by the Research Grant Council of the Hong Kong SAR Government on the projects "Second-order and Advanced Analysis of Arches and Curved Structures (PolyU 152012/14E)" and "Second-Order Analysis of Flexible Steel Cable Nets Supporting Debris (PolyU 152008/15E)", by Innovation and Technology Fund of the Hong Kong SAR Government for the project "Development of an energy absorbing device for flexible rock-fall barriers (ITS/059/16FP)" and by the Hong Kong Branch of Chinese National Engineering Research Centre for Steel Construction of The Innovation and Technology Fund of the Hong Kong SAR Government for the project "Advanced Numerical Analyses for Building Structures Using High Performance Steel Materials".

References

Abdalla, K.M. and Chen, W.F. (1995), "Expanded database of semi-rigid steel connections", *Comput. Struct.*, **56**(4), 553-564.

Alhasawi, A., Heng, P., Hjiaj, M., Guezouli, S. and Battini, J.M. (2017), "Co-rotational planar beam element with generalized elasto-plastic hinges", *Eng. Struct.*, **151**, 188-205.

ANSI/AISC360-16 (2016), Specification for Structural Steel Buildings; American Institute of Steel Construction, Chicago, IL, USA.

Artar, M. and Daloglu, A.T. (2015), "Optimum design of Steel Frames with semi-rigid connections and composite beams", *Struct. Eng. Mech., Int. J.*, **55**(2), 299-313.

Bayat, M. and Zahrai, S.M. (2016), "Seismic performance of mid-rise steel frames with semi-rigid connections having different moment capacity", *Steel Compos. Struct., Int. J.*, **25**(1), 1-17.

Cai, J., Liu, Y., Feng, J. and Tu, Y. (2017), "Nonlinear stability analysis of a radially retractable suspen-dome", *Adv. Steel Constr.*, **13**(2), 117-131.

Chan, S.L. (1992), "Large deflection kinematic formulations for three-dimensional framed structures", *Comput. Methods Appl. Mech. Eng.*, **95**(1), 17-36.

Chan, S.L. and Zhou, Z.H. (1994), "Pointwise equilibrating polynomial element for nonlinear analysis of frames", *J. Struct. Eng.*, **120**, 1703.

Chan, S.L. and Zhou, Z.H. (1995), "Second-order elastic analysis of frames using single imperfect element per member", *J. Struct. Eng.*, **121**(6), 939-945.

Chen, W.F. and Kishi, N. (1989), "Semirigid steel beam-to-column connections: Data base and modeling", *J. Struct. Eng.*, **115**(1), 105-119.

Chiorean, C. (2009), "A computer method for nonlinear inelastic analysis of 3D semi-rigid steel frameworks", *Eng. Struct.*, **31**(12), 3016-3033.

Chiorean, C. (2017), "Second-order flexibility-based model for nonlinear inelastic analysis of 3D semi-rigid steel frameworks", *Eng. Struct.*, **136**, 547-579.

CoPSC (2011), Code of practice for the structural use of steel 2011; Buildings Department, Hong Kong SAR Government.

Eurocode 3 (2005), Eurocode 3: Design of Steel Structures: Part 1-1: General Rules and Rules for Buildings.

Farahi, M. and Erfani, S. (2017), "Employing a fiber-based finite-length plastic hinge model for representing the cyclic and seismic behaviour of hollow steel columns", *Steel Compos. Struct., Int. J.*, **23**(5), 501-516.

Gao, L., Jiang, K., Bai, L. and Wang, Q. (2017), "Experimental study on stability of high strength steel long columns with box-sections", *Adv. Steel Constr.*, **13**(4), 399-411.

Gu, J.X. and Chan, S.L. (2005), "Second-order analysis and design of steel structures allowing for member and frame imperfections", *Int. J. Numer. Methods Eng.*, **62**(5), 601-615.

Hoang, V.L., Dang, H.N., Jaspart, J.P. and Demonceau, J.F. (2015), "An overview of the plastic-hinge analysis of 3D steel frames", *Asia Pacific J. Comput. Eng.*, **2**(1), 4.

Iu, C.K. (2016a), "Generalised element load method with whole domain accuracy for reliable structural design", *Adv. Steel Constr.*, **12**(4), 466-486.

Iu, C.K. (2016b), "Nonlinear analysis of the RC structure by higher-order element with the refined plastic hinge", *Comput. Concrete, Int. J.*, **17**(5), 579-596.

Iu, C.K. and Bradford, M. (2012a), "Higher-order non-linear analysis of steel structures, Part I: Elastic second-order formulation", *Adv. Steel Constr.*, **8**(2), 168-182.

Iu, C.K. and Bradford, M. (2012b), "Higher-order non-linear analysis of steel structures, Part II: Refined plastic hinge formulation", *Adv. Steel Constr.*, **8**(2), 183-198.

Kim, S.E. and Choi, S.H. (2001), "Practical advanced analysis for semi-rigid space frames", *Int. J. Solids Struct.*, **38**(50), 9111-9131.

King, W.S., White, D.W. and Chen, W.F. (1992), "Second-order inelastic analysis methods for steel-frame design", *J. Struct. Eng.*, **118**(2), 408-428.

Kishi, N., Chen, W., Goto, Y. and Hasan, R. (1996), "Behavior of tall buildings with mixed use of rigid and semi-rigid connections", *Comput. Struct.*, **61**(6), 1193-1206.

Lezgy-Nazargah, M. and Kafi, L. (2015), "Analysis of composite steel-concrete beams using a refined high-order beam theory", *Steel Compos. Struct., Int. J.*, **18**(6), 1353-1368.

Liew, J.Y.R., White, D.W. and Chen, W.F. (1993a), "Second-order refined plastic-hinge analysis for frame design. Part I", *J. Struct. Eng.*, **119**(11), 3196-3216.

Liew, J.Y.R., White, D.W. and Chen, W.F. (1993b), "Second-order refined plastic-hinge analysis for frame design. Part II", *J. Struct. Eng.*, **119**(11), 3217-3236.

Liew, J.Y.R., Chen, H., Shanmugam, N.E. and Chen, W.F. (2000), "Improved nonlinear plastic hinge analysis of space frame

structures", *Eng*. *Struct*., **22**(10), 1324-1338.
Lui, E.M. and Chen, W.F. (1987), "Steel frame analysis with flexible joints", *J*. *Constr*. *Steel Res*., **8**, 161-202.
Liu, S.W., Liu, Y.P. and Chan, S.L. (2014a), "Direct analysis by an arbitrarily-located-plastic-hinge element — Part 1: Planar analysis", *J*. *Constr*. *Steel Res*., **103**, 303-315.
Liu, S.W., Liu, Y.P. and Chan, S.L. (2014b), "Direct analysis by an arbitrarily-located-plastic-hinge element — Part 2: Spatial analysis", *J*. *Constr*. *Steel Res*., **103**, 316-326.
Nguyen, P.C. and Kim, S.E. (2013), "Nonlinear elastic dynamic analysis of space steel frames with semi-rigid connections", *J*. *Constr*. *Steel Res*., **84**, 72-81.
Nguyen, P.C. and Kim, S.E. (2016), "Advanced analysis for planar steel frames with semi-rigid connections using plastic-zone method", *Steel Compos*. *Struct*., *Int*. *J*., **21**(5), 1121-1144.
Saritas, A. and Koseoglu, A. (2015), "Distributed inelasticity planar frame element with localized semi-rigid connections for nonlinear analysis of steel structures", *Int*. *J*. *Mech*. *Sci*., **96-97**, 216-231.
Thai, H.T. and Kim, S.E. (2015), "Second-order distributed plasticity analysis of steel frames with semi-rigid connections", *Thin-Wall*. *Struct*., **94**, 120-128.
Thai, H.T., Kim, S.E. and Kim, J. (2017), "Improved refined plastic hinge analysis accounting for local buckling and lateral-torsional buckling", *Steel Compos*. *Struct*., *Int*. *J*., **24**(3), 339-349.
Torbaghan, M.K., Sohrabi, M.R. and Kazemi, H.H. (2018), "Investigating the behavior of specially pre-fabricated steel moment connection under cyclic loading", *Adv*. *Steel Constr*., **14**(3), 412-423.
Vogel, U. (1985), "Calibrating frames", *Stahlbau*, **10**, 295-301.
White, D.W. (1993), "Plastic-hinge methods for advanced analysis of steel frames", *J*. *Constr*. *Steel Res*., **24**(2), 121-152.
White, D.W., Jeong, W.Y. and Toğay, O. (2016), "Comprehensive stability design of planar steel members and framing systems via inelastic buckling analysis", *Int*. *J*. *Steel Struct*., **16**(4), 1029-1042.
Yang, L., Zhao, M.h., Chan, T.M. and Shang, F. (2018), "Flexural buckling design of fabricated austenitic and duplex stainless steel columns", *Adv*. *Steel Constr*., **14**(2), 184-205.
Yau, C.Y. and Chan, S.L. (1994), "Inelastic and Stability Analysis of Flexibly Connected Steel Frames by Springs-in-Series Model", *J*. *Struct*. *Eng*.*-Asce*, **120**(10), 2803-2819.
Zhang, H., Ellingwood, B.R. and Rasmussen, K.J. (2014), "System reliabilities in steel structural frame design by inelastic analysis", *Eng*. *Struct*., **81**, 341-348.
Zhang, X., Rasmussen, K.J. and Zhang, H. (2016), "Second-order effects in locally and/or distortionally buckled frames and design based on beam element analysis", *J*. *Constr*. *Steel Res*., **122**, 57-69.
Zhou, Z.H. and Chan, S.L. (1995), "Self-equilibrating element for second-order analysis of semirigid jointed frames", *J*. *Eng*. *Mech*.*-Asce*, **121**(8), 896-902.
Ziemian, R.D. and Abreu, J.C.B. (2018), "Design by advanced analysis–3D benchmark problems: Members subjected to major-and minor-axis flexure", *Steel Constr*., **11**(1), 24-29.
Zohra, D.F. and Abd Nacer, I.T. (2018), "Dynamic analysis of Steel Frames with semi-rigid connections", *Struct*. *Eng*. *Mech*., *Int*. *J*. **65**(3), 327-334.